Received 21 May 2025; revised 9 July 2025; accepted 26 July 2025. Date of publication 31 July 2025; date of current version 19 August 2025.

Digital Object Identifier 10.1109/OJCOMS.2025.3594489

Design of SIMO *M*-QAM System for Ultrasonic Communications on Shallow Waters

UNAI FERNÁNDEZ-PLAZAOLA, FRANCISCO J. CAÑETE (Senior Member, IEEE), EDUARDO MARTOS-NAYA, AND LUIS DÍEZ

Communications and Signal Processing Lab, Telecommunication Research Institute, E.T.S.I. Telecomunicacion, Universidad de Malaga, 29010 Malaga, Spain

CORRESPONDING AUTHOR: U. FERNÁNDEZ-PLAZAOLA (e-mail: unai@uma.es)

This work was supported in part by the European Regional Development Fund, and in part by the Spanish Government under Project PID2023-147914OB-I00.

ABSTRACT In this work, we present a transmission system that uses single-carrier modulation *M*-ary symbols quadrature amplitude modulation (*M*-QAM) for underwater acoustic communications (UAC) in the ultrasonic band. It exploits the diversity that four hydrophones provide at reception in a single-input multiple-output (SIMO) 1×4 configuration and also includes, for each stream, a phase-locked loop (PLL) for synchronization and a turbo-equalization subsystem, with fractionally-spaced equalizer (FSE) and decision feedback equalizer (DFE) filters, adaptive by means of least mean squares (LMS) algorithm, both of which are driven by an low-density parity check (LDPC) decoder decisions. The paper describes the system design and analyze its performances on trials carried out on shallow waters of the Mediterranean sea. Achievable data rates exceeding 200 kb/s between links of transmission distances longer than 200 m are obtained with a satisfactory low bit-error rate (BER).

INDEX TERMS Adaptive filter, diversity, equalization, fading channels, LMS, MIMO, modem design, measurements, QAM, PLL, synchronization, underwater acoustic communications, wireless channels, wireless communications.

I. INTRODUCTION

ACOUSTIC waves represent an interesting option among other for underwater wireless communications. The UAC channel, compared to the one when optical waves are used, has less attenuation, is not affected by water turbidity and has not misalignment problems [1], [2], [3]. However, the UAC channel presents difficulties, since it has a high temporal and frequency dispersion [4]. Time dispersion due to the multipath effect, especially in shallow water. Frequency dispersion because, although the medium and the communication terminals may have little movement, they result in a pronounced Doppler due to the low propagation speed of sound in water. Furthermore, achieving high transmission rates requires maximize the used bandwidth and as the carrier frequency is comparable, results in a wideband behavior. All these difficulties make obtaining high data rates in UAC a challenge.

A. LITERATURE REVIEW

In the pioneering works [4], [5], coherent digital modulation were employed for transmission experiments of UAC over deep and shallow waters with carrier frequencies in the audio band. Later, with the irruption of orthogonal frequency-division multiplexing (OFDM) as the mainstream transmission technique for wireless communications, in UAC the interest was also put on multi-carrier modulation [6]. Not only OFDM but also other variants have been proposed such as orthogonal time frequency space (OTFS) [7] or filter bank multicarrier (FBMC) [8]. However, the demand for higher data rates together with the adverse features of the acoustic channel [9], [10], especially in shallow waters, has fostered a threefold strategy: first, to widen the bandwidth by moving up the frequencies towards the ultrasonic range [11]; second, to extend the initial systems that were single-input single-output (SISO) to other multi-antenna configurations (multi-hydrophones in this case) either multiple-input multiple-output (MIMO) or SIMO to improve the received signal to noise ratio (SNR); and third, to renew the attention to single-carrier modulations like quadrature amplitude modulation (QAM) and phase-shift keying (PSK) [12], [13], [14], [15], [16], [17], [18], [19], [20], [21], [22], [23]. The latter is due, mainly, to the long

© 2025 The Authors. This work is licensed under a Creative Commons Attribution 4.0 License.
For more information, see https://creativecommons.org/licenses/by/4.0/

impulse response of the UAC channel and its high selectivity in both frequency and time, which represents a challenge for multi-carrier techniques since leads to long cyclic prefix with low efficiency and significant distortion caused by the channel time variation during the long OFDM symbols.

We have developed an underwater acoustic measurement system [24] that has allowed us to conduct campaigns in the Mediterranean Sea. With the obtained measurements we have validated narrowband channel models [25] or characterized wideband channels [11]. In addition, we have developed a preliminary transmission system based on OFDM [26], traditionally considered the simplest scheme in terms of the complexity of the channel estimation and compensation, compared to other single-carrier schemes. Now, in this paper, we present a single-carrier based solution that offers some advantages: it has lower efficiency loss due to both the high number of pilots that are needed in OFDM for channel estimation and synchronization and the long cyclic prefixes required to avoid intersymbol interference (ISI). In Section I-C we justify in more detail the interest of single-carrier schemes versus OFMD.

The system we present has a SIMO (1x4) configuration, since the equipment availability does not allow to increase the number of transmitters. The eventual scalability of this set-up toward a full MIMO system, e.g., to a 2x2 or 2x4, would increase the system complexity and represent an interesting challenge. The main problem is the unavailability of channel state information (CSI) at the transmitter but still a better diversity gain, and a reliability improvement, can be expected by transmitting only one independent data stream from the two projectors by exploiting combination techniques of the increased number of MIMO streams. More complex systems have been proposed in [18], [19], where also MIMO multiplexing is exploited by sending several independent data sequences from the transmitters, over the same experimental campaign. In these valuable works, more sophisticated equalization strategies are studied looking for a better performance, with a MIMO channel estimation, obtained from orthogonal-in-time training sequences periodically sent from the set of transmitters, and channel compensation by means of a bank of FSE-DFE to mitigate both the ISI and the inter-channel interference, in [18], or a single FSE-DFE receiver but with iterative processing, in [19]. This strategy leads to an incremental efficiency loss due to longer training sequences w.r.t. data sequences that can be compensated for the higher spectral efficiency provided by the MIMO multiplexing gain. The trials were conducted in a band between 27 and 50 kHz, lower and narrower than the one employed in this proposal. Thus, they achieve lower data rates but with higher spectral efficiency, and over deeper waters with a depth between 120m and 90m. The channel in this latter scenario, as explained in Section I-B, is expected to exhibit a better behavior with less multipath effect. On the other hand, using a narrower band or a better channel than the one proposed here can also benefit filter adaptation. When using MIMO multiplexing, the number of equalizer coefficients to be adapted increases by the number of sequences multiplexed by the transmitter, which reduces the channel variation tracking capability of the filters by the same factor. This will have a more limiting effect on wider bandwidths and higher ultrasonic frequencies or on channels affected by a greater multipath effect, as it worsens the structure of the channel impulse response.

B. ON THE SPECIAL CHARACTERISTICS OF HORIZONTAL LINKS IN SHALLOW WATERS

The tough characteristics of UAC channels worsen when using horizontal links in shallow waters because they exhibit a stronger multipath propagation effect than both the vertical ones and the links in deeper waters [9], [10], [11], [25]. Multipath is caused by the reflections of the acoustic signal on the seabed, the surface of the sea and any other objects. In horizontal links, apart from the direct or line-of-sight (LoS) component, there is a strong reflection on the sea surface (due to the large difference between the characteristic impedance of seawater and air), another weaker one at the bottom, whose amplitude depends on the nature of the seabed, and subsequent higher order reflections on these surfaces and other ones on objects according to the scenario. If the bottom is sandy, a significant part of the incident energy is usually absorbed, and the reflections are weaker than if the bottom is rocky, when the effect is more similar to the one in the sea surface. In general, the channel of vertical links is more favorable for communication than the horizontal one, since other multipath components than the LoS, which are orthogonal to both the surfaces at the top and the bottom, usually reach the receiver in a smaller number, with lower energy and less temporal dispersion.

Regarding the channels established in deep waters, these are also better for communication since the non-LoS components the travel longer distances and experience notable attenuation due to the signal absorption, because part of the signal energy is transferred to the medium, and signal spreading. Consequently, the performance observed in the proposed system, over shallow waters near the coast with sandy bottom, will be much less favorable than the one expected if the channel is established in deeper waters or over more vertical links. More unfavorable conditions could only be found with a rocky seabed.

C. ON THE SUITABILITY OF OFDM VS SINGLE-CARRIER SCHEMES IN UAC

Different from what is the common practice in radio wireless systems, in UAC ones there is a renaissance of using single-carrier modulation schemes. Actually, there are many works devoted to single carrier techniques like [12], [13], [14], particularly, in the remarkable paper by Rudander et al. in [14], the authors state that most of the high-speed systems for UAC are single carrier. We have collected some of the references therein: in [15], [16], [17], [18], [19] QPSK modulation is employed; while in [20], 8-PSK; in [21],

16-QAM; and in [22], [23], it is 64-QAM, the selected modulation.

One of the advantages always highlighted of OFDM systems is their simplicity to deal with frequency selective and time-varying channels, for instance regarding the equalization part, compared to the computational complexity of single-carrier ones. However, it is worth mentioning that for the relative low data rates involved in UAC systems, this is not a so relevant factor. Another significant feature for focusing on OFDM in radio wireless is the ability to use adaptive modulation and coding schemes quite efficiently. To guarantee the latter, a good knowledge of the CSI in the transmitter is required, which is provided by an agile enough feedback channel. Nevertheless, this feedback is not practical in most UAC systems, at least not through an underwater acoustic link, due to the low propagation speed of the sound together with the short coherence time of the channel, because of its strong time variation.

The hostile nature of UAC channels, with a very long impulse response and a significant double selectivity in both time and frequency, which makes them to exhibit large spread factors (delay spread multiplied by the Doppler spread) represents a challenge for multi-carrier techniques. On the one hand, the long cyclic prefix required to compensate for the long channel impulse response leads to long OFDM symbol, and significant distortion, in the form of intercarrier interference (ICI), appears due to the channel time variation during the symbol period. On the other hand, the spectral efficiency in OFDM is severely affected for both the long cyclic prefix and the loss in pilot subcarriers needed to yield a good estimation of the very frequency-selective channel. To give an example of this latter problem, our single-carrier proposal offers an efficiency loss of approximately a 10% without coding, due to the training sequence in each data frame, as will be explained later. According to our on-going OFDM system design for the same UAC scenarios, it is very difficult to achieve an efficiency loss as low as 10% with the long cyclic prefix and the density of pilot subcarriers required.

For all the reasons mentioned above, and unlike wireless radio links, single-carrier must not be discarded in UAC in favor of OFDM, especially in shallow water horizontal links.

D. CONTRIBUTIONS

The objective of this work is to construct a system reliable enough to offer relatively high data rates and with a moderate complexity in the realm of ultrasonic UAC in shallow waters. To do so, the transmitted data structure, the algorithms involved in the receiver and the control of its operation has been thoroughly designed after many trials at the sea and an extensive experimental validation. The transmitted signal is generated by direct synthesis in the digital domain different to most other works, e.g., [5], [13], [14], which use an analog up-conversion. This allows to link the carrier and symbol synchronization and simplify these tasks. The main contributions of this proposal are the following ones:

- The design of a 1×4 SIMO receiver with joint adaptive channel equalization and synchronization that includes a bank of PLL, FSE and DFE, which works in a multi-rate configuration and have been properly parameterized for one of the most hostile conditions in UAC channels: horizontal links in shallow waters at the ultrasonic band up to 128 kHz. The equalization scheme differs from the standard by using four DFEs, instead of one as usual [18], providing better tracking capability. In particular, from inspection of the impulse response structure of these shallow water channels, the filter lengths for the FSE and DFE have been reduced as much as possible by making them follow only the variation of the first and main components of the channel response, since the rest vary at a rate that exceeds the adaptive capability of the filters. However, sufficient ISI is removed to maintain good performance when maximal ratio combining (MRC) is applied, despite using only 4 hydrophones. Also, the structure of the SIMO system and the different parameters both in the equalizer filters adaptation, by means of LMS algorithm, and the loop filter of the PLL have been adjusted based on the involved signals characteristics.
- The design of an ad hoc turbo-equalizer system that integrates a channel decoding subsystem, based on LDPC codes, whose decided outputs aid the equalizers adaptation. The operation of this subsystem has been also tailored to the special channel characteristics after thorough experimental testing so that, for instance, the LDPC decoding is bypassed when the risk of entering the error floor region is high.
- The proposal of a frame structure defined according to the size of the LDPC code blocks and customized for the adaptive equalization algorithm. The system operation throughout the training part of the frame is monitored to trigger either a soft training, with a refresh of the filter coefficient adjustment that maintains the channel tracking, or a hard training, with a reset of the filter coefficients and a return to the frame beginning. The decision is based on the supervision of the adaptive filter loop convergence. This control part aims to improve the robustness of the system.
- The evaluation of the designed system and the analysis of its performance with original experimental tests that have been carried out over an extensive set of measurements obtained in sea trials.

E. ORGANIZATION

The paper is organized as follows. The section after this introduction describes the transmission system and the frames structure. In Section III, the receiver algorithms and the details of their design are explained. Section IV addresses the system evaluation on a set of actual measured channels and, finally, in the last section, some conclusions are drawn.

II. TRANSMISSION SYSTEM DESCRIPTION

The communication system was developed with signal processing techniques over a flexible programmable hardware. It is prepared to work in real time on actual scenarios with signal transmission, link quality monitoring and signal recording at reception. Afterwards, additional offline processing is performed on the recorded received signal for receiver full operation and for system performance evaluation.

The setup employed for this work is a hardware/software UAC platform that has been described in [24]. It essentially consists of, either in the transmitter or receiver side, the projector or the hydrophones; an analog front-end for signal amplification and transducer adaptation; a digital-to-analog converter (DAC) or analog-to-digital converter (ADC) card; and a laptop for signal processing. There are both some real-time signal processing for monitoring the correct measurement progress and other differed-time ones for the receiver operation and performance analysis. The UAC platform can be used for different purposes, such as channel sounding, noise registering, or the transmission of several kinds of modulated signals (multicarrier or single carrier), but here we only focused on the functionality of emulating a *M*-QAM transmission system.

We propose here to synthesize the band-pass signal at the ultrasonic range directly in the digital domain, since the required sampling frequency is lower enough. This way, the symbol period and carrier frequency are linked, which allows a joint synchronization at the receiver.

In addition, there are two operation modes in the system: with channel coding, to increase reliability, or without it, to increase spectral efficiency. When the coding mode is selected, the information bits are encoded using LDPC codes before mapping them to the *M*-QAM constellation.

A. TRANSMITTER PART

The transmitter part consists of a hardware with: laptop, which yields the sounding signals for channel characterization or the data frames for communication; a digital acquisition board that performs the digital to analog conversion, with a sampling frequency of up to 1 MHz and a resolution of 16 bits; a power amplifier and a hydrophone used as a projector. An ad-hoc software application has been developed to manage and control the trials.

B. RECEIVER PART

The receiver part consists of a hardware with: four hydrophones; each one followed by a pre-amplifier; which feeds a channel of the two digital acquisition boards, that perform the analog to digital conversion, with a sampling frequency of 500 kHz, which is enough to convert directly the band-pass signal, and a resolution of 16 bits; and a laptop, for the incoming signal recording and the monitoring software.

C. TRANSMISSION FRAME STRUCTURE

The equivalent low-pass representation of the *M*-QAM signal used for transmission is given by

$$x(t) = \sum_n a_n g(t - nT), \tag{1}$$

where $\{a_n\}$ are the *M*-ary complex symbols of the constellation set, T is the symbol period and $g(t)$ is the basic pulse that we select to have a root raised-cosine spectrum.

The data for communication is organized in frames, or packets, that consist of three virtual parts, whose sizes are given in *M*-QAM modulated symbols:

1) The first one (P1), of 200 symbols, which is used for an initial synchronization phase.
2) The second one (P2), of 2000 symbols that includes also the P1 ones, which is employed for the training period of adaptive filters. This part of the frame is uncoded.
3) And the third one (P3), of 18144 symbols, which corresponds to the payload and can be encoded.

Hence the size of the entire frame is 20144 *M*-QAM symbols with an overhead of the preamble part P2 w.r.t. the payload part P3 close to 10%. This number of symbols is adjusted to the size of LDPC encoded blocks, which are of 648 bits, i.e., 324 symbols for 4-QAM or 162 for 16-QAM, and, therefore, the payload part P3 contains either 56×324 4-QAM symbols, or 112×162 16-QAM symbols.

We refer to these parts of the frame as virtual in the sense that all frame symbols carry *M*-QAM symbols after mapping pseudo-random bits that, depending on the desired receiver configuration, can be considered as known preambles or as random information data to be detected. For this purpose, we use the binary dithering technique explained in [27] that allows the flexibility of making modifications of the error correction coding post-experiment while the transmitted symbol sequence remains unchanged. We have chosen this frame structure heuristically, after different tests, because this technique allows us to play with the different parts and modify which one corresponds to the preamble or the payload. Hence, the frames have 20144 symbols ($2000+56\times324$) at a baud rate of $1/T$=62500 symbols/sec, which leads to an approximate frame duration of 322 ms.

D. FRAME MONITORING

Since the channel is strongly time-varying in UAC at shallow waters, adaptive equalization is required, which uses iterative algorithms that can be unstable and not to converge. Hence, the organization in frames makes the system more robust. A frame integrity monitoring procedure has been designed to select between two equalization adaptation strategies and to label defective frames.

The frames can be started either using a soft training or a hard training. In the soft one, the equalizer filters internal state is conserved from the last frame and a new training begins, whereas in the hard one, the equalizer filters internal state is reset to zero and both a new

initial synchronization phase and the equalization training are started. The reasoning underneath this procedure is that, although the time-varying channel may have changed significantly, the adaptive algorithms convergence may be faster by training them from the last channel state than from the initial state, with zero coefficients.

For the first frame only a hard training is possible. For the following ones, by default, the systems works with the soft training and, during the first 20 symbols of this phase, the error between the equalizer output and the correct value of the transmitted symbols, which is known, is monitored. If the mean squared value of this error exceeds a heuristic threshold, then a hard training is restarted and the previous frame is marked as defective, since we have found that this situation is reached in events with significant performance degradation when the equalization system becomes unstable. Assuming that the symbols are normalized to have a unit mean-square value, the above threshold for detecting whether or not to restart a hard training is set to 0.25. This selection is based on experimental observations of the mean squared error for many realizations of received signals of both defective and correct frames. The value, after averaging the error for 20 symbols, defines a very clear boundary between the two situations and it is quite independent of the channel conditions and does not need to be adapted.

III. RECEIVER DESIGN

The signal processing algorithms designed for the receiver start with the first stage for initial synchronization and is performed over the P1 part of the frame whose values are known and considered here as a preamble. It has a threefold purpose: to locate the frame beginning, by means of an threshold detector; the estimation of received signal power; and to achieve a coarse sampling synchronization, which is carried out by maximizing the cross-correlation of the received signal with the transmitted pulse.

The second stage comprises essentially the demodulation, equalization and detection functions, and constitutes the most challenging part of the design. In Fig. 1, a diagram of the structure of this stage is shown. The main elements have the following functionality: demodulation of band-pass waveform to get its equivalent low-pass signal; re-sampling for fine signal synchronization, aided by a PLL of the second type and second order; equalization, with both a FSE and a DFE; and M-QAM decision device. Additionally, the receiver works with a SIMO configuration 1×4 and hence, many of the receiver blocks are implemented four times in parallel for the signal chain from each hydrophone. A MRC block is included prior to decision that enhances the M-QAM constellation symbols by taking advantage of the spatial diversity that the SIMO structure provides.

The subsystems that appear inside the dashed green line rectangle, in Fig. 1, work with an N_o oversampling factor w.r.t to the symbol rate and the discrete-time index is k, the ones inside the dashed orange line rectangle work at twice the symbol rate and their discrete-time index is m, the remaining subsystems work synchronously with the symbol rate and their discrete-time index is n.

The nominal sampling frequency at the receiver is $f_s = 500 \cdot 10^3$, and the normalized symbol frequency is given by

$$\Omega_o = \frac{f_o}{f_s} = \frac{1}{N_o}, \tag{2}$$

where f_o is the symbol frequency and N_o is an integer number that represents the oversampling factor. Hence, the normalized carrier frequency is

$$\Omega_c = \frac{f_c}{f_s}, \tag{3}$$

being f_c the carrier frequency in Hz. Since the sampling frequency at the transmitter is synchronized with the carrier frequency, by the transmitter design, if f_s is synchronized at the receiver, then Ω_c is constant and does not depend on the oscillator jitter.

For the explanation herein, which describes the second stage, the input signal is considered the received signal in the time interval that has been determined in the first stage of initial synchronization. We denote this signal as $r_l[k]$, with an actual sampling rate $\hat{f}_s$, where l is the spatial index $l \in \{1, \ldots, L\}$ and L is the number of SIMO receivers.

A. DOWN-CONVERSION AND PHASE-LOCKED LOOP

Let's consider one of the l SIMO receivers to illustrate the signal processing chain. The input signal excites firstly an analytic band-pass filter, which acts also as anti-aliasing filter, before down-sampling by a factor $N_o/2$, so that the FSE receives a signal up-sampled by 2. The shape of such filter is not critical, for the purpose of aliasing avoidance and out-of-band noise removal, but we select it to be the response of a raised-cosine spectrum, which is the same as the basic pulse.

Therefore, the input signal is filtered according to

$$s_l[k] = \sum_{d=0}^{D_{FILT}} r_l[k-d]h[d], \tag{4}$$

where $h[k]$ is the analytical filter impulse response. The demodulated signal after the down-conversion is

$$q_l[k] = s_l[k]e^{-j2\pi k\Omega_c}. \tag{5}$$

The re-sampler is driven by a second order discrete-time PLL and yields the reference symbol rate interpolated by two. The PLL consists of a phase detector, a filter loop of second order and a numerically-controlled oscillator (NCO). The phase detector compares the signal before detection with the decided symbols. The re-sampler block has a threefold functionality: re-sampling, decimation by a $N_o/2$ factor and carrier frequency error compensation. It is worth mentioning that we denote the discrete-time index as k before resampling and with m and n afterwards, which correspond to the blocks operating at twice the symbol-rate and to the symbol

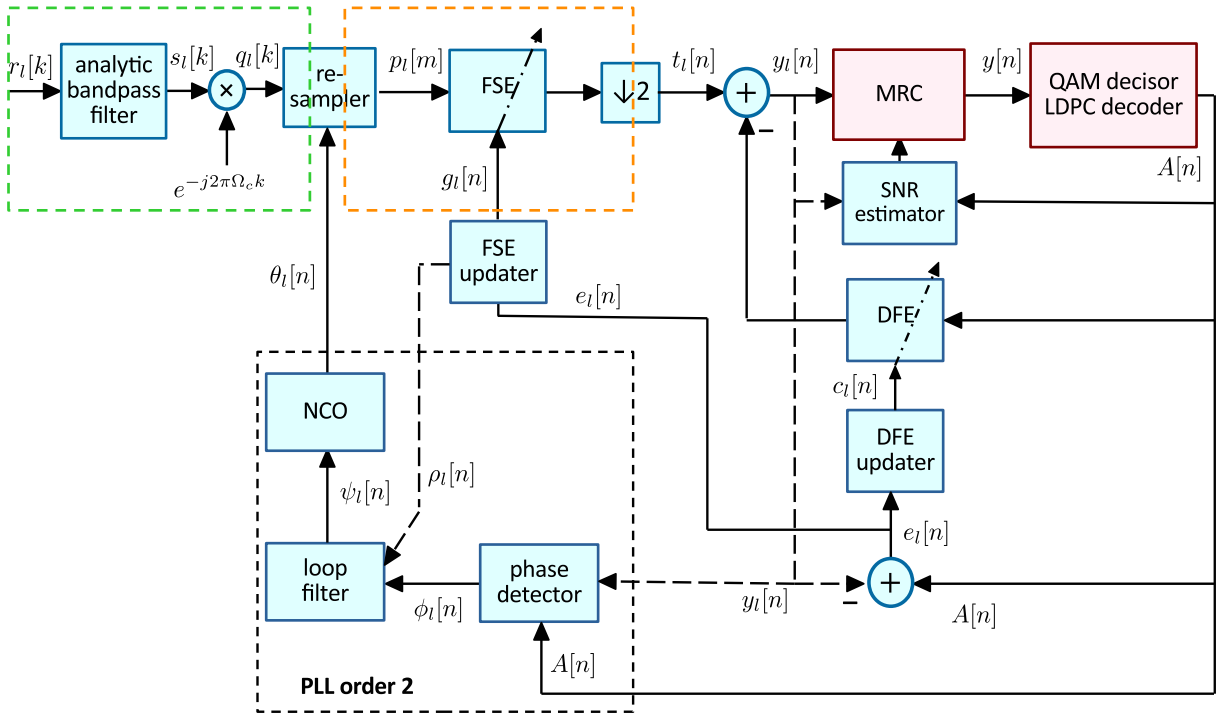

FIGURE 1. Diagram of the receiver structure. The elements with light blue background are implemented four times in parallel, each for one of the SIMO 1x4 streams, the ones with light red background are unique.

rate, respectively. The equations that rule the re-sampler subsystem are

$$\begin{aligned} p_l[2n] &= \big\{q_l\big[nN_o/2 + i_l[n]\big] \cdot \mu_k[n] \\ &\quad + q_l\big[nN_o/2 + i_l[n] - 1\big] \cdot (1 - \mu_l[n])\big\} \\ &\quad \cdot e^{-j2\pi\theta_l[n]\Omega_c}, \\ p_l[2n+1] &= \big\{q_l\big[N_o/2(n+1) + i_l[n]\big] \cdot \mu_k[n] \\ &\quad + q_l\big[N_o/2(n+1) + i_l[n] - 1\big] \cdot (1 - \mu_l[n])\big\} \\ &\quad \cdot e^{-j2\pi\theta_l[n]\Omega_c}. \end{aligned} \tag{6}$$

Two samples are calculated for each value of n because the m discrete-time index of the $p_l[m]$ signal has an oversampling factor of 2 w.r.t. the symbol rate. An integer shift, $i_l[n]$, is compensated by a sample delay or advance of the signal, whereas the fractional shift, $\mu_l[n]$, is compensated by a linear interpolation between two successive samples and both are obtained from the output of the PLL, given later in (12) and (13). In addition, a phase rotation term, according to $\theta_l[n]$, given later in (11), is included to compensate for the residual synchronization error in the carrier frequency that has been used in the down-conversion. Such error is derived from the sampling frequency error because f_s and f_c are linked as stated in (3).

Regarding the PLL, at the input of the phase-detector block, two signals arrive (for each SIMO stream): $y_l[n]$ and $A[n]$, given later by (15) and (22). The estimation of the residual phase error of the symbols is

$$\phi_l[n+1] = \angle\big\{y_l[n]A^*[n]\big\}. \tag{7}$$

The input to the loop filter also includes a term $\rho_l[n+1]$ to decouple the FSE effect on the timing error, as described in the next section in (19). Both contributions are combined as

$$\eta_l[n+1] = \phi_l[n+1] + \beta\rho_l[n+1], \tag{8}$$

where constant β is set to 0.25. The PLL operation is described by these two equations:

$$\psi_l[n+1] = \psi_l[n] + \alpha\eta_l[n+1], \tag{9}$$

which yields the loop filter output and

$$\Delta\Omega_l[n+1] = \psi_l[n+1] + \sqrt{\alpha}\eta_l[n+1], \tag{10}$$

which yields the frequency deviation for the NCO. Constant α is fixed to 10^{-4} for the first 500 symbols in hard training and is halved for the rest of symbols and for the whole symbols in soft training. Therefore, the NCO output yields the sampling error

$$\theta_l[n+1] = \theta_l[n] + \Delta\Omega_l[n+1]. \tag{11}$$

We obtain the integer and fractional part of the sampling error from

$$i_l[n+1] = \lfloor -\theta_l[n+1] \rfloor, \tag{12}$$

and

$$\mu_l[n+1] = -\theta_l[n+1] - i_l[n+1], \tag{13}$$

respectively.

B. EQUALIZATION AND MRC

As above mentioned, the receiver contains two linear equalizers for the channel compensation: a FSE and a DFE. The former operates at a rate of two samples per symbol period, while the latter is synchronous with the symbol rate, i.e., with one sample per symbol period. The FSE is an efficient implementation of an adaptive filter that combines the functions of a matched filter and a synchronous equalizer and, hence, it is a realization of the optimum linear receiver [28].

The FSE operation which, besides the filtering, performs a decimation by a factor of 2 is given by

$$t_l[n] = \sum_{d=0}^{D_{FSE}} p_l[2n-d] g_l^{(n)}[d]. \tag{14}$$

The number of coefficients chosen for the FSE is D_{FSE}=29. The equalized output of the FSE is improved by the use of a DFE [28]. This improvement is based on the fact that, assuming that prior decisions are correct, we are subtracting the effect of preceding decisions on the current sample. The DFE operation is described by

$$y_l[n] = t_l[n] - \sum_{d=1}^{D_{DFE}} A[n-d] c_l^{(n)}[d] \tag{15}$$

The number of coefficients of the DFE is set to D_{DFE}=400 samples.

Both equalizers are adaptive, with decision-driven adjustments (after down-sampling the FSE output by two) that is carried out by the LMS algorithm [29]. The operation of this algorithm is defined by the equation for the adjustment of the adaptive filters coefficients at iteration $\mathbf{n}$ depending on the error signal $e_l[n]$, in the form

$$g_l^{(\mathbf{n}+1)}[d] = g_l^{(\mathbf{n})}[d] + \gamma_F p_l[n-d] e_l^*[n] \tag{16}$$

$$c_l^{(\mathbf{n}+1)}[d] = c_l^{(\mathbf{n})}[d] + \gamma_D A[n-d] e_l^*[n] \tag{17}$$

where $()^*$ denotes conjugation, γ_F and γ_D are the FSE and DFE updating constants, respectively, and the filter coefficients range is $d = 0, 1, \ldots, D_{FSE} - 1$, and $d = 0, 1, \ldots, D_{DFE} - 1$, respectively. The estimated signal is given by $p_l[n]$ in (6) for the FSE and by $A[n]$ in (22) for the DFE. The error signal is calculated in both cases as

$$e_l[n] = D[n] - y_l[n], \tag{18}$$

being the desired signal $D[n]$, at the beginning of the adaptive filters operation a preamble, a sequence of known symbols that are transmitted during the so-called training period. Afterwards, this signal is taken from the decided M-QAM symbols in (22), $D[n] = A[n]$ and, hence, the filter adaptation is decision-driven.

The length of the equalization training period is set to 2000 samples approximately (P2) and the step size γ is selected according to different criteria. For the DFE, it is the inverse of the filter length, i.e., $\gamma_D = D_{DFE}^{-1}$, and it is invariant. While, for the FSE, it is $\gamma_F = (\hat{P}_{in} D_{FSE})^{-1}/2$, where $\hat{P}_{in}$ denotes the estimation of the input signal power, and this constant is reduced by a factor of 16 after 500 symbols, a quarter of the training period. These values are selected in a heuristic manner to find a balance between the adaptation convergence speed and the remaining error floor.

Finally, there is an estimation of the timing error that is absorbed by the FSE, given by

$$\rho_l[n+1] = \left\{ \sum_{d=D_{FSE}/2+1}^{D_{FSE}} \left(g_l^{(n)}[d] \right)^2 - \sum_{d=0}^{D_{FSE}/2-1} \left(g_l^{(n)}[d] \right)^2 \right\} \Big/ \sum_{d=0}^{D_{FSE}} \left(g_l^{(n)}[d] \right)^2, \tag{19}$$

which is used in the PLL block as indicated earlier.

Afterwards, the signals of each SIMO sub-channel are combined to gain diversity with MRC. This latter technique requires knowledge of the signal SNR that is estimated aided by the decision as well, to increase the precision. The MRC combination is done according to

$$y[n] = \frac{\sum_{l=1}^{L} y_l[n] \hat{SNR}_l[n]}{\sum_{l=1}^{L} \hat{SNR}_l[n]}, \tag{20}$$

where an estimation of the SNR is obtained by means of

$$\hat{SNR}_l[n+1] = \frac{E_A}{\frac{1}{P} \sum_{d=0}^{P-1} |e_l[n-d]|^2}, \tag{21}$$

being E_A the mean energy of the constellation symbols.

This design differs from the standard of a SIMO or MIMO receiver like the one described in [18] since we adapt the coefficients of four DFE aided by four different error signals, comparing before the MRC processing, rather than using one DFE and one error signal obtained after the MRC. This difference accelerates the convergence of filter adaptation and thus improves the ability to track the channel time variation, the most limiting factor in this type of channel.

C. DECISION AND CHANNEL DECODING

Finally, the M-QAM decision is taken and it can be either a hard-decision or a soft-decision one, depending on the system configuration: of whether LDPC decoding is applied afterwards or not. The decision device operation can be represented as

$$A[n] = F(y[n]) \tag{22}$$

where $F(x)$ corresponds to the decision function. As seen before, there is a feedback of the decided output to the equalizers adaptive control, the phase detector and the SNR estimator. When the system is configured with channel coding, turbo-equalization is performed with a LDPC channel decoder. For this purpose, the selected code is a quite common one, as specified for IEEE 802.11n/ac/ax standard ([30], Subclause 19.3.11.7). This LDPC code offers when using a code-rate Rc=3/4 with 4-QAM signals over an

TABLE 1. System parameters.

Subsystem	Parameter	Description
SIMO	$N_{rx} = 4$	number of streams
	MRC	combination technique
Signal generation	$f_c = 80$kHz	center frequency
	$B \in \{32, 128\}$kHz	bandwidth
	$1/T \in \{31.25, 62.5\}$kHz	symbol frequency
	$f_s = 500$kHz	sampling frequency
	$N_o \in \{8, 16\}$	oversampling factor
Modulation	$M \in \{4, 16\}$	M-QAM constellation size
	root raised-cosine	pulse shape
	$\alpha = 0.4$	roll-off factor
	$N_p = 97$	pulse length (samples)
LDPC coding	$n = 648$	encoded block size
	$k \in \{540, 486, 324\}$	input block size
	$R_c = k/n \in \{5/6, 3/4, 1/2\}$	code rate

additive white Gaussian noise (AWGN) channel, a BER-post (i.e., after decoding) of approximately 10^{-5} for a SNR of 6dB, and below 10^{-9} for SNR greater than 7.5 dB.

As previously explained, the encoded block size has been selected of 648 bits, which corresponds to 324 symbols in 4-QAM and to 162 symbols in 16-QAM. The code rate value can be chosen from among 5/6, 3/4 and 1/2 that leads to the input block size depicted in Table 1. The LDPC decoding is made with soft-decision by means of the belief propagation algorithm [31] and, for this purpose, a log-likelihood ratio (LLR) metric must be provided for each of the decided bits. This metric for the k-ith bit, considering that the actual noise at the receiver is of Gaussian nature and taking into account only the nearest points in the M-QAM constellation, can be simplified to

$$LLR(b_k) \simeq \frac{1}{2\sigma_n^2}\left(\min_{s\in\mathcal{S}_1}\|q-s\|^2 - \min_{s\in\mathcal{S}_0}\|q-s\|^2\right) \quad (23)$$

where q is the received M-QAM noisy symbol; σ_n is the noise standard deviation; and s is the correct symbol that can belong to either $\mathcal{S}_0$ or $\mathcal{S}_1$, which are the sets of constellation symbols where the bit b_k is 0 and 1, respectively.

The procedure for implementing turbo-equalization comprises two steps for each encoded block. In the first step, no channel decoding is performed, the symbols $A^{(1)}$ are obtained by hard-decision and used to feed back the equalizing filters. At the end of the block, the LLR values obtained are used to make a soft-decision with LDPC and new $A^{(2)}$ symbols are obtained. In a second step, a return to the beginning of the block is done, by loading signals and filter coefficients to the corresponding values, and the system now works using the $A^{(2)}$ symbols as decision to feed back the equalizing filters. Once the block end is reached, the updated LLR values are used to obtain the final decided symbols $A^{(3)}$ with the LDPC decoder. Eventually, if the symbols $A^{(2)}$ are equal to $A^{(1)}$, the second step is skipped.

TABLE 2. Set of measured links.

Channel index	Approx. distance (m)
1,2,3	83
4,5,6,7	162
8,9,10	309

IV. SYSTEM EVALUATION OVER REAL MEASUREMENTS

In this section, the performance achieved for a set of UAC links and the transmission system configuration is studied. A brief description of the measured scenarios and the set-up are given first.

A. TRIALS DESCRIPTION

The measured channels used for this work were registered in shallows waters in the Mediterranean sea (in the coast of Malaga, Spain). The links were established in horizontal UAC scenarios between two boats at different distances and the projector and hydrophones were submerged at 6 m from the sea level which had a depth ranging from 12 m and 20 m. The selected bandwidth was within the 3-octave ultrasonic band from 32 kHz to 128 kHz. A large set of measurements has been made for different distances between boats, ranging from 50m to 400m. The following are the results of a set that we consider to be most representative: 10 channels which are listed in Table 2. The distance between boats, despite there were anchored, is approximated due to the location measure uncertainty and the sea motion during the measurement duration. The four hydrophones at the receiver side were arranged in a vertical array with 1 meter separation among them (that is, their depths were 3, 4, 5, 6 m). The duration of the useful signal transmission measurement for each link was approximately of one minute (there was some extra preparatory measurements for the system monitoring and control).

TABLE 3. Bit rate in kb/s.

Modulation	4-QAM	16-QAM
nominal	125	250
preamble	112.6	225.2
LDPC 5/6	93.8	187.6
LDPC 3/4	84.4	168.9
LDPC 5/6	56.3	112.6

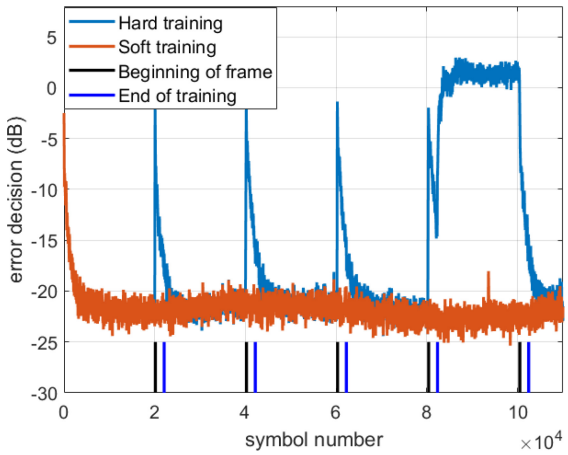

FIGURE 2. Evolution of the equalization MSE in time at the receiver in one of the SIMO 1x4 streams for the two adaptation strategies.

B. SYSTEM PERFORMANCE EVALUATION

The performance of the designed system in the actual channels is addressed here. First, table 3 shows a summary of the bit rate achieved by the system after the reduction due to the overhead introduced by the preamble for equalization adaptation and the LDPC redundancy for the different code rates.

Next, the behavior of the frame transmission and the receiver adaptation is studied. In Fig. 2, a plot of the equalizer operation is given for a measured channel, with an illustrative purpose. The two different approaches of the adaptive equalization, with soft and hard training, are compared. It is observed the evolution of the mean squared error (MSE), but smoothed with a moving average of 50 symbols, which exhibits a decreasing curve during adaptation.

The first approach corresponds to the hard training, in the blue line, in which a new synchronization is carried out and a reset of the adaptive filter coefficients is done systematically for each transmitted frame. In this case, the error increases at the beginning of each frame and decreases until convergence is reached. The second one corresponds to the soft training, in the red line, in which the filter coefficients of the previous frame are maintained as a starting point for the adaptation at each frame (hence, a training phase with the filter coefficients zeroed is only done when transmission starts). It can be seen that the soft training leads to a more stable system behavior, whereas the hard one exhibits a higher error at each frame beginning and even makes the system not to converge in the last frame, which would be lost.

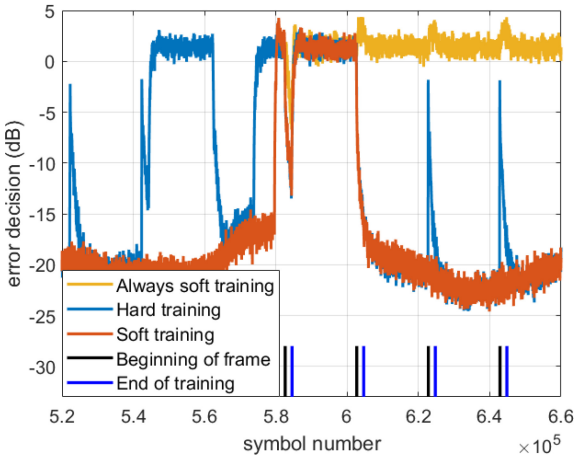

FIGURE 3. Evolution of the equalization MSE in time at the receiver, in a different test to the one in Fig. 2, in other channel and showing a case where no hard training is ever applied.

As explained in Section II-D, a frame monitoring procedure has been implemented and the proposed strategy is to do soft training by default in all frames but, if the equalizer error gets too high a hard training is started, and the previous frame is marked as defective. To illustrate this strategy, another test is presented in Fig. 3. As before, the red line, for the soft training, exhibits the best system behavior. Although there is an event of equalizer instability in the third frame, because the channel variation is too severe. Therefore, at the beginning of the fourth frame, a hard training is applied as the third frame is detected as defective. Despite this, the fourth frame is also defective. However, with the hard training of the fifth, the stability is recovered. Alternatively, the systematic hard training case, in the blue line, exhibits that also the second frame is lost. An additional curve is shown, in the orange line, which corresponds to the case in which a hard training is never performed. As observed, when the equalization loop gets off the stable zone the error is not controlled anymore and all the subsequent frames are lost.

The frame monitoring performance is evaluated in the following Figures 4 and 5. The frames can be classified in three groups: correct frames, without any symbol errors; few-errors frames, with some symbol errors but without equalization system instability issues; and defective frames, in which the equalizer convergence is lost or never reached. In the figures, the occurrence rate of correct and defective frames is studied, in both cases with or without applying channel coding. A code rate of 5/6 is applied in the channel coding case.

Fig. 4 shows these results for 4-QAM and also the average SNR of the received signal in two points: after the bandpass filter, i.e., $s_l[k]$ and after the MRC block, i.e., $y_l[n]$. The values of the latter are worse because they also contain distortion and ISI due to imperfect channel response compensation, hence we denote it as signal to noise, interference and distorsion ratio (SNDR). These values are

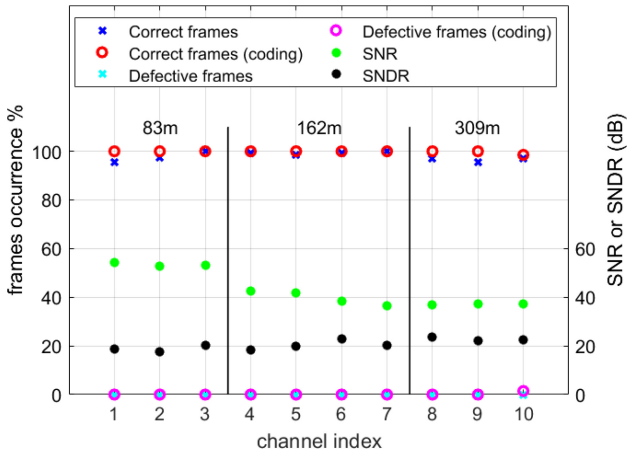

FIGURE 4. Frame events representation for the set of channels using 4-QAM. The SNR at the receiver input and the SNDR at the equalizer output are also shown. Channels are ordered by transmission distance.

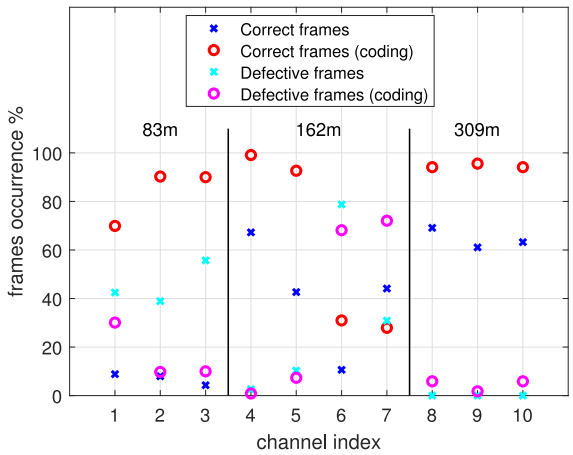

FIGURE 5. Frame events representation for the set of channels using 16-QAM. Channels are ordered by transmission distance.

not included in Fig. 5 because the tendencies are similar and their inclusion would impair readability. As can be seen, good results are obtained for 4-QAM. In almost all situations, 100% correct frames are achieved and only in some cases this value is not reached, specially when channel coding is not used.

Fig. 5 offers results for 16-QAM, which are clearly worse than those for 4-QAM, because a 16-QAM constellation requires more than 20dB of SNR, over an AWGN channel, to achieve a BER of 10^{-5}. As shown in Fig. 4, the SNDR does not exceed 20dB in some links. Except for channels 6 and 7, which will be discussed later, the improvement that LDPC provides is very noticeable. Furthermore, comparing the results of channels 1, 2 and 3 with those of channels 8, 9 and 10, it may be surprising that for shorter distances, despite having a higher SNR, the results are worse, but this is due to they have a lower SNDR. This is due to the fact that the geometry of the different reflections at the surface and bottom of the sea produces a faster time-variation of the channel response over shorter distance links, making more challenging the equalizer filters adaptation.

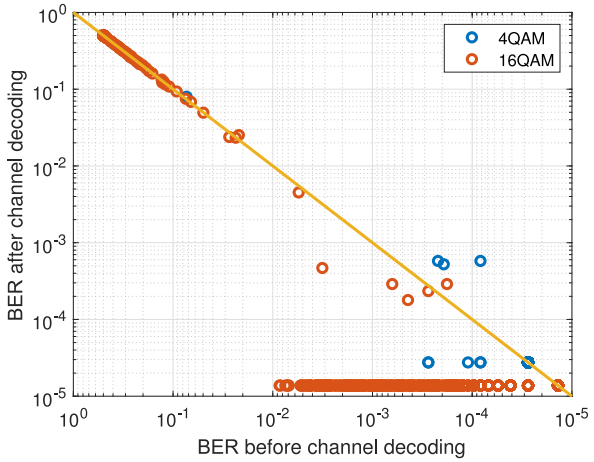

FIGURE 6. BER comparison before and after LDPC channel decoding at the receiver.

Let us now analyze the results for channels 6 and 7 in Fig. 5. Clearly, channel coding worsens the performance of correct frames. We propose changing the implementation of turbo equalization to improve these results. For a better understanding let's first study the performance of turbo equalization and its interaction with the equalization filters adaptation. For this purpose we use the following metrics: the BER without coding, i.e., computing it previous to the LDPC decoder and the BER after decoding. We continue using a code rate of 5/6. In Fig. 6, the relationship between these two metrics can be observed for the entire set of frames of all channels. Each point corresponds to one frame and the yellow line, which indicates the same BER before and after, is plotted as a reference. A BER floor appears that is due to the frame length and leads to an upper bound of the BER when there are no errors. In general, it is observed the expected improvement of the coding (lower-right part of the plot) but in some frames there is a worsening, i.e., points above the yellow line. In these cases the turbo equalization is counterproductive, since the wrong decisions in LDPC decoding are fed back to the equalizer filters, resulting in propagation errors.

In order to reduce the problem explained, we propose the following change to turbo equalization implementation. If comparing the symbols $A^{(2)}$ obtained with LDPC decoding with the initial ones $A^{(1)}$, they differ in a number of symbols greater than a selected threshold, the $A^{(2)}$ symbols are discarded and are not fed back to the equalizers, i.e., step 2 of turbo equalization is not performed. The selected threshold, which is related to the error correcting capability of the selected code, has been fixed to 20 symbols, a value that will be justified later. Fig. 7 presents the same metrics as Fig. 6 but applying the discarding proposal. It should be noted that it is not possible to make a correspondence between points in Fig. 6 and points in Fig. 7. For example, if for the same channel, a frame is defective with one approach but not with

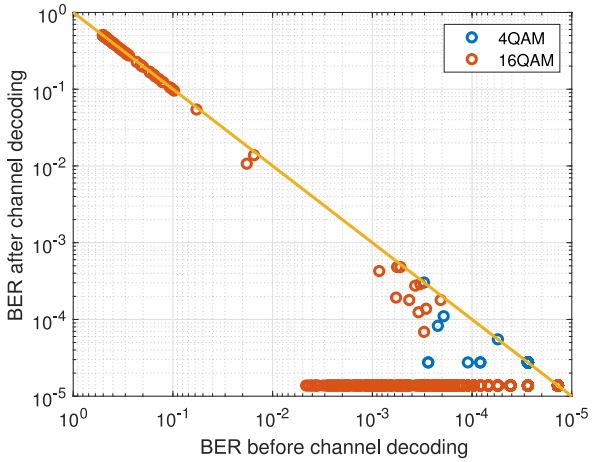

FIGURE 7. BER comparison before and after LDPC channel decoding at the receiver by applying the discarding proposal.

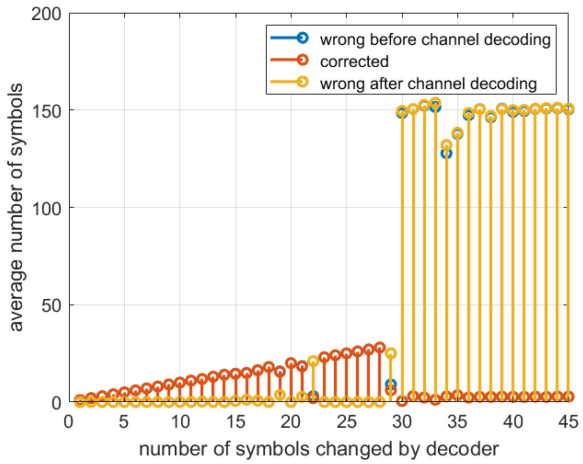

FIGURE 8. The average number of symbols in each decoding block for all frames that were wrong before decoding and were either corrected or remained wrong after decoding.

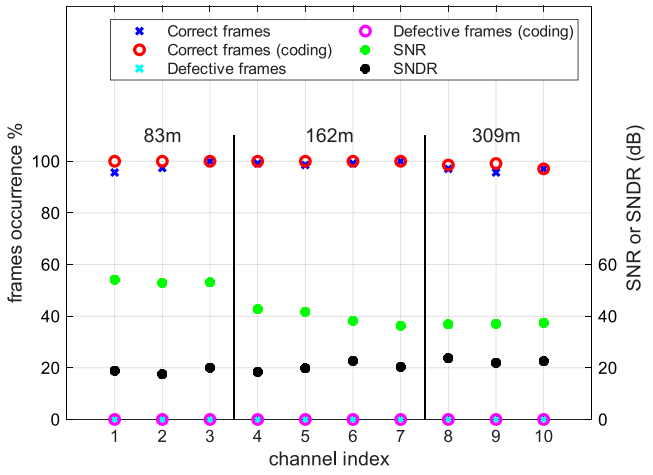

FIGURE 9. Frame events representation for the set of channels using 4-QAM by applying the discarding proposal. The SNR at the receiver input and the SNDR at the equalizer output are also shown. Channels are ordered by transmission distance.

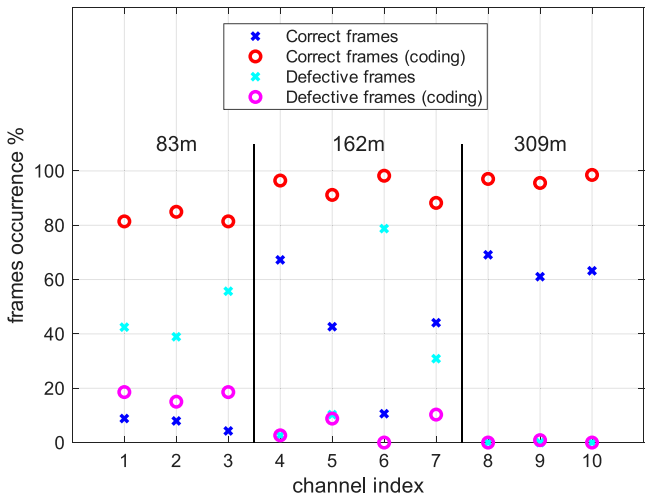

FIGURE 10. Frame events representation for the set of channels using 16-QAM by applying the discarding proposal. Channels are ordered by transmission distance.

the other, then the evolution of the rest of the frames will be totally different for each approach, giving points in the figures with different coordinates. Therefore, the comparison of the two figures must be made in global terms. As can be seen, in Fig. 7 there are no situations in which channel coding worsens the results, i.e., there are no points above the yellow line. On the other hand, the number of dots in the upper left part is higher in Fig. 6 than in Fig. 7. These results suggest that the achievable performance of correct frames with this discarding proposal should improve.

We have selected the threshold value of 20 to deactivate the LDPC decoding based on experimental tests. Figure 8 illustrates those tests for all the channels. It shows a study of the decoder behavior and its impact on the receiver performance, in particular a classification of the symbols in a decoding block is done according to three categories: symbols that are wrong before decoding, which can be assessed since we know the real transmitted ones, in blue; symbols that have been corrected by the LDPC decoder, in red; and symbols that remain wrong after decoding, in yellow. The abscissa is the number of symbols that have been changed by the decoder and the ordinate is the average number in each category for all the blocks of all the channels. As can be seen, except for one case for 22 symbols, the LDPC decoder behavior is satisfactory up to around 25 changed symbols, from this point on the decoder starts to fail and becomes counterproductive. For this reason, we have selected a conservative threshold of 20 symbols modified by the decoder to avoid its operation or not.

Figures 9 and 10 present the same results as Figures 4 and 5 but using the proposal of discarding LDPC decoded symbols when there are many corrections in a block. As can be seen, the results for 4-QAM are nearly the same, but it is worth noting that now there are no defective frames on any channel. The improvement is very notable in 16-QAM, since LDPC significantly enhances the

performance of channels 6 and 7. In addition, in almost all other channels, the results are better.

V. CONCLUSION

This paper revisits single-carrier systems for UAC in shallow water links at the ultrasonic band, since the strong selectivity these channels have both in time and frequency compromises the performance of OFDM, the mainstream technique in current systems. For this purpose, a *M*-QAM system in a SIMO 1×4 configuration, with LDPC channel coding that includes a receiver with a PLL and two adaptive equalizers, FSE and DFE, has been selected, with a careful design of the signal processing algorithms tailored to the underwater channel characteristics. It also incorporates novel parts aiming to a more robust and reliable system like: an ad-hoc frame structure suited to the channel time variations; a control of the frames to trigger a reset of the equalization adaptation and a new synchronization procedure; a turbo-equalization subsystem where equalization adaptation is aided by the LDPC decoder decisions, with loop monitoring and control. The developed system exhibits a noteworthy performance for such hostile channels, which has been illustrated with several tests over real measured channels in the Mediterranean sea, which represent themselves a valuable technical result.

We have focused on solutions with limited complexity that can be competitive with current OFDM systems, which boast this feature. In the end, the expected trade-off appears of better performance vs. system complexity. In this sense, the equalizer sub-system design for this SIMO configuration aims to partially compensate for the ISI by adapting only the most relevant components of the time-varying channel impulse response, thereby preventing a significant increase in the number of filter coefficients. Consequently, the system is mostly interference-limited rather than noise-limited. This explains why the observed performance is not very sensitive to the SNR, unless it is too low. An interesting, and not too complex, alternative to be explored, aiming at improving the system performance by taking a MIMO advantage over SIMO, is the use of space-time coding with two independent data streams, e.g., with the Alamouti scheme for a 2x2 system, which yields diversity without the need of a feedback channel to get CSI at transmitter [32]. Further work is planned to improve the equalization subsystem by using some other algorithms like the recursive least squares (RLS) and to construct a real-time prototype based on this design, aiming at applications of underwater video transmission either for surveillance, with cameras, or exploration aided by drones or remotely operated vehicles.

REFERENCES

[1] M. Salman, J. Bolboli, R. P. Naik, and W.-Y. Chung, "Aqua-sense: Relay-based underwater optical wireless communication for IoUT monitoring," *IEEE Open J. Commun. Soc.*, vol. 5, pp. 1358–1375, 2024.

[2] A. Das, R. Atta, B. Pal, N. Sarkar, S. Santra, and A. S. Patra, "14 Gbps QAM–OFDM optical wireless communication system employing pulse shaping technique in coastal water environment with optimization of cyclic prefix length," *J. Opt.*, vol. 1, pp. 1–10, Dec. 2024. [Online]. Available: https://doi.org/10.1007/s12596-024-02435-3

[3] A. Huang, L. Tao, and Y. Niu, "Underwater wireless optical MIMO system with spatial modulation and adaptive power allocation," *Opt. Commun.*, vol. 412, pp. 21–27, Apr. 2018. [Online]. Available: https://www.sciencedirect.com/science/article/pii/S0030401817311124

[4] M. Stojanovic, J. A. Catipovic, and J. G. Proakis, "Phase-coherent digital communications for underwater acoustic channels," *IEEE J. Ocean. Eng.*, vol. 19, no. 1, pp. 100–111, Jan. 1994. [Online]. Available: https://ieeexplore.ieee.org/document/289455

[5] J. Proakis, M. Stojanovic, and J. Catipovic, "Adaptive equalization algorithms for high rate underwater acoustic communications," in *Proc. IEEE Symp. Auton. Underwater Veh. Technol. (AUV)*, 1994, pp. 157–164. [Online]. Available: https://ieeexplore.ieee.org/document/518620/citations?tabFilter=papers#citations

[6] C. Polprasert, J. A. Ritcey, and M. Stojanovic, "Capacity of OFDM systems over fading underwater acoustic channels," *IEEE J. Ocean. Eng.*, vol. 36, no. 4, pp. 514–524, Oct. 2011.

[7] M. Aldababsa, S. Özyurt, G. K. Kurt, and O. Kucur, "A survey on orthogonal time frequency space modulation," *IEEE Open J. Commun. Soc.*, vol. 5, pp. 4483–4518, 2024.

[8] Y. Zhu, H. Huang, Z. Pu, B. Wang, and Y. Li, "Filter bank multicarrier communication with real part and imaginary part index modulation," *IEEE Open J. Commun. Soc.*, vol. 5, pp. 6201–6211, 2024.

[9] M. Stojanovic and J. Preisig, "Underwater acoustic communication channels: Propagation models and statistical characterization," *IEEE Wireless Commun. Mag.*, vol. 47, no. 1, pp. 84–89, Jan. 2009.

[10] A. C. Singer, J. K. Nelson, and S. S. Kozat, "Signal processing for underwater acoustic communications," *IEEE Commun. Mag.*, vol. 47, no. 1, pp. 90–96, Jan. 2009.

[11] J. López-Fernández, U. Fernández-Plazaola, J. F. Paris, L. Díez, and E. Martos-Naya, "Wideband ultrasonic acoustic underwater channels: Measurements and characterization," *IEEE Trans. Veh. Technol.*, vol. 69, no. 4, pp. 4019–4032, Apr. 2020.

[12] J. Kusuma, A. Jarrot, A. Gelman, A. Croux, and G. Choi, "Pragmatic performance optimization of a multichannel DFE system for a wideband 100 kbps 1-km subsea acoustic modem," in *Proc. 4th Underwater Commun. Netw. Conf. (UComms)*, 2018, pp. 1–4. [Online]. Available: https://ieeexplore.ieee.org/document/8493222

[13] J. Rudander, P. A. Van Walree, T. Husøy, and P. Orten, "Very-high-frequency single-input–multiple-output acoustic communication in shallow water," *IEEE J. Ocean. Eng.*, vol. 44, no. 4, pp. 943–955, Oct. 2019. [Online]. Available: https://ieeexplore.ieee.org/document/8429053

[14] J. Rudander, T. Husøy, P. A. Van Walree, and P. Orten, "Experimental evaluation of a real-time FPGA platform for multichannel coherent acoustic communication," *IEEE J. Ocean. Eng.*, vol. 48, no. 3, pp. 963–972, Jul. 2023.

[15] J. W. Choi, R. J. Drost, A. C. Singer, and J. Preisig, "Iterative multi-channel equalization and decoding for high frequency underwater acoustic communications," in *Proc. 5th IEEE Sens. Array Multichannel Signal Process. Workshop*, 2008, pp. 127–130. [Online]. Available: https://ieeexplore.ieee.org/document/4606839

[16] M. Suzuki, K. Nemoto, T. Tsuchiya, and T. Nakanishi, "Digital acoustic telemetry of color video information," in *Proc. OCEANS*, 1989, pp. 893–896. [Online]. Available: https://ieeexplore.ieee.org/document/586703

[17] P.-P. J. Beaujean, "A performance study of the high-speed, high-frequency acoustic uplink of the HERMES underwater acoustic modem," in *Proc. OCEANS EUROPE*, 2009, pp. 1–6. [Online]. Available: https://ieeexplore.ieee.org/abstract/document/5278282

[18] S. Roy, T. M. Duman, V. McDonald, and J. G. Proakis, "High-rate communication for underwater acoustic channels using multiple transmitters and space–time coding: Receiver structures and experimental results," *IEEE J. Ocean. Eng.*, vol. 32, no. 3, pp. 663–688, Jul. 2007. [Online]. Available: https://ieeexplore.ieee.org/document/4443172

[19] A. Song, M. Badiey, V. K. McDonald, and T. C. Yang, "Time reversal receivers for high data rate acoustic multiple-input–multiple-output communication," *IEEE J. Ocean. Eng.*, vol. 36, no. 4, pp. 525–538, Oct. 2011. [Online]. Available: https://ieeexplore.ieee.org/document/6035995

[20] H. Ochi, Y. Watanabe, T. Shimura, and T. Hattori, "The acoustic communication experiment at 1,600 m depth using QPSK and 8PSK," in *Proc. OCEANS MTS/IEEE SEATTLE*, 2010, pp. 1–5. [Online]. Available: https://ieeexplore.ieee.org/abstract/document/5664308
[21] A. Kaya and S. Yauchi, "An acoustic communication system for subsea robot," in *Proc. OCEANS*, 1989, pp. 765–770. [Online]. Available: https://ieeexplore.ieee.org/document/586677
[22] C. Pelekanakis, M. Stojanovic, and L. Freitag, "High rate acoustic link for underwater video transmission," in *Proc. Oceans Celebr. Past Teaming Toward Future*, 2003, pp. 1091–1097. [Online]. Available: https://ieeexplore.ieee.org/document/1283454
[23] J. Younce, A. Singer, T. Riedl, B. Landry, A. Bean, and T. Arikan, "Experimental results with HF underwater acoustic modem for high bandwidth applications," in *Proc. 49th Asilomar Conf. Signals, Syst. Comput.*, 2015, pp. 248–252. [Online]. Available: https://ieeexplore.ieee.org/document/7421124
[24] U. Fernández-Plazaola, J. López-Fernández, E. Martos-Naya, J. F. Paris, and F. J. Cañete, "HW/SW platform for measurement and evaluation of ultrasonic underwater communications," *Sensors*, vol. 22, no. 17, p. 6514, 2022. [Online]. Available: https://www.mdpi.com/1424-8220/22/17/6514
[25] F. J. Cañete et al., "Measurement and modeling of narrowband channels for ultrasonic underwater communications," *Sensors*, vol. 16, no. 2, p. 256, 2016. [Online]. Available: http://www.mdpi.com/1424-8220/16/2/256
[26] P. Cobacho-Ruiz, F. J. Cañete, E. Martos-Naya, and U. Fernández-Plazaola, "OFDM system design for measured ultrasonic underwater channels," *Sensors*, vol. 22, no. 15, p. 5703, 2022. [Online]. Available: https://www.mdpi.com/1424-8220/22/15/5703
[27] S. Yang, G. B. Deane, J. C. Preisig, N. C. Sevüktekin, J. W. Choi, and A. C. Singer, "On the reusability of postexperimental field data for underwater acoustic communications R&D," *IEEE J. Ocean. Eng.*, vol. 44, no. 4, pp. 912–931, Oct. 2019.
[28] R. D. Gitlin, J. F. Hayes, and S. B. Weinstein, *Data Communication Principles*. New York, NY, USA: Plenum, 1992.
[29] S. Haykin, *Inglés Adaptive Filter Theory*, 5th ed. Upper Saddle River, NJ, USA: Pearson, 2014.
[30] *International Standard—Telecommunications and Information Exchange Between Systems–Specific Requirements for Local and Metropolitan Area Networks–Part 11: Wireless LAN Medium Access Control (MAC) and Physical Layer (PHY) Specifications*, ISO/IEC/IEEE Standard 8802-11:2022E, Oct. 2022. [Online]. Available: https://ieeexplore.ieee.org/document/9930960
[31] R. G. Gallager, *Low-Density Parity-Check Codes*. Cambridge, MA, USA: MIT Press, 2003. [Online]. Available: https://mitpress.mit.edu/9780262571777/low-density-parity-check-codes/
[32] A. Goldsmith, *Wireless Communications*. Cambridge, U.K.: Cambridge Univ. Press, 2005.

UNAI FERNÁNDEZ-PLAZAOLA received the M.Sc. and Ph.D. degrees in telecommunication engineering from the University of Málaga. Since 1997, he has been with the Department of Ingeniería de Comunicaciones, University of Málaga, where he is currently an Associate Professor. His doctoral thesis was on precise positioning in global navigation satellite systems. His teaching activities include communications and image and video processing. His doctoral thesis was on precise positioning in global navigation satellite systems. His current research interests include performance analysis, adaptive modulation, and signal processing in digital communication systems, in radio wireless and underwater communications.

FRANCISCO J. CAÑETE (Senior Member, IEEE) received the M.S. and Ph.D. degrees in telecommunication engineering from the Universidad de Málaga (UMA), Spain, in 1996 and 2004, respectively.

In 1996, he was with the Empresa Nacional de Ingenieria y Tecnologia (INITEC), Instrument and Control Department, working in the design of power plants. In 1997, he was with Alcatel Spain, Research and Development Department, working in the design of wireless local loop systems. In 1998, he joined the Department of Ingeniería de Comunicaciones, UMA, where he is currently an Associate Professor. From 2000 to 2001, he collaborated with the Nokia System Competence Team in Málaga, developing radio resource management algorithms for cellular systems. He has served at UMA in different responsibilities as: the Head of Department, the Deputy Vice-Chancellor for Academical Organization, a Vice-Rector of Studies, and the Vice-Dean of the ETSI Telecomunicación. His research is focused on signal processing for communication systems and, in particular, on channel modeling and the design of transmission techniques for applications of wireless systems, underwater acoustic communications, and power line communications.

EDUARDO MARTOS-NAYA received the M.Sc. and Ph.D. degrees in telecommunication engineering from the University of Málaga, Spain, in 1996 and 2005, respectively. In 1997, he joined the Department of Communication Engineering, University of Málaga, where he is currently a Professor. His research activity includes digital signal processing for communications, channel estimation, synchronization and performance analysis, and channel modeling of wireless systems.

LUIS DÍEZ received the M.S. and Ph.D. degrees in telecommunications engineering from the Universidad Politécnica de Madrid (UPM), Spain, in 1989 and 1995, respectively.

From 1987 to 1997, he was with the Signals, Systems and Radiocommunication Department, UPM as an Assistant Professor. Since 1997, he has been with the Communication Engineering Department, Universidad de Málaga, where he is currently an Associate Professor. His research interests are primarily in digital communications. His experience includes most of its applications, such as voice-band, DSL, and cable modems; satellite, mobile, and power line communications; and technical aspects, such as synchronization, adaptive signal processing, modulation, coding, and multiple access.